Article:
Auer, S (2017) Simple Model of the Effect of Solution Conditions on the Nucleation of Amyloid Fibrils. The Journal of Physical Chemistry B, 121 (38). pp. 8893-8901. ISSN: 1520-6106

https://doi.org/10.1021/acs.jpcb.7b05400

A Simple Model of the Effect of Solution Conditions on the Nucleation of Amyloid Fibrils

Stefan Auer

School of Chemistry, University of Leeds, Leeds LS2 9JT, United Kingdom

*Corresponding author: s.auer@leeds.ac.uk

ABSTRACT

It is well known that peptide and protein fibrillation is strongly affected by the solution conditions, but a fundamental understanding of how amyloid fibril nucleation depends on solution pH, salt concentration and solvent is absent. Here we use expressions from Debye-Hückel theory to describe the interactions between charged amino-acids in combination with our recently developed non-standard nucleation theory to predict the concentration dependence of the fibril nucleation rate under different solvent conditions. The general rule that emerges from these considerations is that changes in solution pH, salt concentration and solvent that increase the bonding energy between the fibril building blocks decrease the fibril solubility and promote fibril nucleation, in line with experimental observations. The simple analytical relations between the nucleation rate, the fibrils solubility and the binding energies provide a tool to control and understand amyloid fibril formation by changing the solution conditions.

INTRODUCTION

Proteins when dissolved in aqueous solution that contain salt form a polyelectrolyte solution. Because amino acids contain ionisable groups, the predominant ionic form of these molecules in solution depends on the pH. The interactions between the amino acids of the proteins depend on their partial charges, but also on the concentrations of the ions in solution, which shield the interactions between charged amino acids, and

the solvent, as a change in the dielectric constant will affect the electrostatic screening between charged residues. Understanding the effects of solution pH, salt and solvent on the solubility and nucleation rate of amyloid fibrils is important e.g. for biomedical applications because proteins need to function under physiological conditions [1].

Solution conditions can strongly affect the kinetics and mechanism of amyloid fibril formation as well as their morphology. A prominent example is the aggregation of amyloid β peptide related to Alzheimer's disease for which there is an optimum pH range for fibril formation and the fibril morphology is strongly pH dependent (see, e.g. Ref. [2-5]). A strong pH dependence has been reported for numerous other proteins including β_2-microglobulin [6], gelsolin [7], HypF N-terminal domain [8], transthyretin [9], α-synuclein [10], prion protein [10], SH3 domain [11], major cold-shock protein [12] and the ABri peptide [13]. For example in the case of α-synuclein it has been shown [10] that the aggregation lag time increases with solution pH and decreases with the addition of salt, and its fibrillation rate can be changed by orders of magnitude when the pH is changed by only a few tenths of a unit [14].

To obtain a quantitative understanding of how the interactions between the proteins depend on the solvent conditions and their assembly behavior is challenging. The (overall) charge of the protein seems to be a central parameter. For example the removal of a single charged amino acid can shift the pH dependence by a full unit [15], and the concentration above which monomeric peptides aggregate correlates with its overall charge [16]. More generally it has been shown [17] that the pH at maximal fibril formation correlates with the pH dependence of the protein solubility (but not stability) and is near the isoelectric point, where the protein is expected to be least soluble. The important role of charge has been used to design peptides in which pH can be used [18,19] as a reversible switch for the formation of hydrogels.

Theoretical approaches to provide insight into solvent effects on amyloid fibrillation include models that use physiochemical properties of the protein to predict their aggregation propensities [20-23], and rate equations to analyze protein fibrillation experiments [24,25], but they differ to our approach in that they do not provide information about the fibril solubility and the nucleation rate. Molecular simulations using a full atomistic description of proteins have been used to investigate protein aggregation (see e.g. recent review by Morriss-Andrews and Shea [26]), but they are restricted to simulations of self-assembly of a few peptide fragments and short times.

Using simplified models it has been possible to perform larger scale simulations, but studying solvent effects on protein aggregation is notoriously difficult [26].

The objective of this work is to apply our newly developed nucleation model [27-29], in combination with Debye-Hückel theory to describe the interactions between charged amino acids, to predict how the solvent affects the fibril solubility, the threshold concentration below which fibril formation becomes biologically irrelevant, and the nucleation rate. In particular, our considerations pertain to changes in (i) the solution pH, (ii) salt concentration, and (iii) the solvent. As in our previous work [29], the emphasis of this work is to reveal the general principles that underlie the fibril nucleation and for this reason we apply our theoretical framework to a model peptide system rather than a specific protein.

METHOD

Fraction of ionised groups. Every peptide has two titratable groups at the N- and C-terminal residues and the side chain groups when they are composed of one (or several) of the following seven amino acids: histidine, lysine, arginine, aspartate, glutamate, cysteine, and tyrosine. During titration with a strong base, the titratable groups of a peptide lose their protons in a stepwise manner. At low pH the carboxylate group is uncharged whereas the ammonium group is protonated and has a charge +1. When base is added, the carboxyl group loses its proton to become a negatively charged carboxylate group around $\mathrm{pH} \approx 2.3$. As more base is added, the side chain groups of the titratable amino acids lose their proton at their characteristic pKa values, and adding additional base results in the ammonium ion losing its proton to become a uncharged carboxylate group at $\mathrm{pH} \approx 9.7$. Although the titration and pKa values of all individual amino acids are known and tabulated, the pKa values of these amino acids differ from those of free amino acids because they are affected by their microenvironment. The pH-dependence of the fraction of ionised groups can be calculated by using the Henderson-Hasselbach equation and is given by

$$f = \frac{1}{1+10^{\mp pH \pm pK_a}} \qquad (1)$$

where the exponent – pH + pK_a is used if the titratable group becomes charged with increasing pH, whereas + pH – pK_a when it becomes charged with decreasing pH.

Debye-Hückel theory. Our consideration of the electrostatic interactions between charged amino acids is based on Debye-Hückel theory, within the dimensionless potential of an amino acid at distance *r* is given by

$$eV(r)/kT = \mp\frac{\lambda_B}{r}\exp\left(-r/\lambda_D\right)f \qquad (2)$$

Here *e* is the elementary charge, *k* the Boltzmann factor, *T* the temperature, *V* the dimension-bearing potential, and f is the fractional charge of the titratable group as given in Eq. (1) above. The Bjerrum length $\lambda_B = e^2/4\pi\varepsilon_0\varepsilon_r kT$ is the length at which the electrostatic interaction between two elementary charges is comparable to the thermal energy kT and ε_0 is the permittivity in vacuum. For water with a dielectric constant $\varepsilon_r = 80$ and at $T = 300$ K it is given by $\lambda_B = 0.7$ nm. The Debye length $\lambda_D = \sqrt{\varepsilon_0\varepsilon_r kT/e^2\sum_i c_i z_i}$ is a measure for the electrostatic screening in the solution where the concentrations c_i of salt ions of type *i* in solution is in units of mol/l (or mol/m^3). In a 1:1 electrolyte where the charge of all ions is $z_i = 1$, the expression simplifies to $\lambda_D = \sqrt{\varepsilon_0\varepsilon_r kT/e^2 N_A 2C}$ where N_A is Avogadro's number and the salt concentration *C* is in moles per m^3. For example λ_D for 1 mol/m^3 (1 mM) and 100 mol/m^3 (100 mM) salts in water are 10 nm and 1 nm, respectively. This corresponds to an ionic strength *I* of 1mM and 100 mM, respectively, typically used in experiments on protein aggregation.

The effect of solvent on pKa value. The dissociation constant of a standard dissociation reaction $\mathrm{HA} \rightleftarrows \mathrm{H^+ + A^-}$ is given by $K_a = \frac{[\mathrm{H^+}][\mathrm{A^-}]}{[\mathrm{HA}]} = \frac{[\mathrm{A^-}]^2}{[\mathrm{HA}]}$, where we have used that the concentration of cations, $[\mathrm{H^+}]$, and anions, $[\mathrm{A^-}]$, in a 1:1 electrolyte are equal. On the simplest level the effect of solvent on the pKa value may be considered by the difference in coulomb energy, $\Delta u \approx e^2/\left(4\pi\varepsilon_0\varepsilon_r\left(a_+ + a_-\right)kT\right)$, on separating two monovalent ions from contact in a solvent with dielectric constant ε_r, where a_+ and a_- are the radii of the cation and anion, respectively. The concentration of dissociated ions in solution is then given by[30],

$X_S \approx \exp(-\Delta u / kT) = \exp\left[-\frac{e^2}{4\pi\varepsilon_0\varepsilon_r\left(a_+ + a_-\right)kT}\right]$ and the value of this dimensionless parameter may be identified as the solubility of the monovalent ions in any solvent, in mole-fraction units. As the dissociation constant K_a is proportional to X_s, it follows that K_a is proportional to $e^{-\text{const}/\varepsilon_r}$, or

$$pK_a = -\log_{10} K_a \propto -\log_{10} X_s \propto 1/\varepsilon_r \,. \qquad (3)$$

This relation predicts that the pK_a values in non-polar solvents are higher than in water. While the derived relation is far to simple to quantitatively account for the pK_a dependence for amino acids in different solvents, it has been shown to predict trends for monovalent salts and amino acids reasonably well (see e.g. Fig. 3.3 of Ref. [30]).

Fibril model. In our model system [27,28,31] we assume that each peptide is composed of 10 amino acids. In the fibril the peptide is in an extended β-strand conformation and each amino acid can form bonds with nearest neighbour amino acids only (Fig.1). We denote ε the binding energy of amino acids between two-nearest neighbour β-strands in a β-sheet that form hydrogen bonds, ε_h is the binding energy of amino acids that form hydrophobicity mediated bonds, and ε_c is the binding energy due to columbic bonds between neighbour β-strands. The dimensionless specific surface energy of the 1β-sheet face perpendicular to the β-sheet lengthening axis can then be written as

$$\psi = n\alpha + n_h\alpha_h - n_c\alpha_c \qquad (4)$$

where $\alpha = \varepsilon / 2kT$, $\alpha_h = \varepsilon_h / 2kT$ and $\alpha_c = \varepsilon_c / 2kT$ are the dimensionless specific surface energies per amino acid at the 1β-sheet ends due to hydrogen, hydrophobic and columbic bonds, respectively. The n's are the corresponding numbers of such bonds of the amino acids at the 1β-sheet ends. While hydrogen and hydrophobicity mediated bonds are attractive, columbic bonds are repulsive, which is taken into account by the minus sign in eq. 4. Similarly, the dimensionless specific surface energy of the 1β-sheet face parallel to the β-sheet lengthening axis can be written as

$$\psi_h = n_h\alpha_h - n_c\alpha_c \qquad (5)$$

Note, that in this expression we do not consider the contribution of possible hydrogen bonds between side-chains.

To provide insight into the effect of pH on the formation of amyloid fibrils we assume that a peptide has only one titratable group (Fig. 1), and that only the side chain of this group can be either in a protonated or deprotonated state at pH values which are either below or above its nominal pKa value (note that this implies that the titratable carboxylate and ammonium group at the N- and C-terminal residues are not considered in our model). Furthermore, we assume that the hydrogen and hydrophobicity mediated bonding is the same for all amino acids. The dimensionless specific surface energies ψ and ψ_h from Eqs. 4 and 5 can then be calculated by considering that each peptide in the fibril can form $n = 10$ hydrogen bonds between two nearest neighbour β-strands in a β-sheet, and $n_h = 10$ hydrophobicity mediated bonds between any two nearest neighbour β-strands. As each peptide has only one titratable group, the number of columbic bonds $n_c = 1$. The values used for the interactions energies are $\varepsilon = 2\ kT$ (a typical hydrogen bonding energy measured experimentally [32]) so that $\alpha = \varepsilon / 2kT = 1$, $\varepsilon_h = 0.2\ kT$ (a value for the hydrophobic interactions often used in protein simulations [33]) so that $\alpha_h = \varepsilon_h / 2kT = 0.1$. While these two bond energies are constant, the columbic bond energy between two charged amino acids is described by the Debye Hueckel potential, eq. 2, and depends both on distance between the amino acids and the solution conditions (i.e. pH, salt concentration). Assuming that the peptides within the fibril are arranged parallel, the distance between the neighboring amino acids in a β-sheet is 0.48 nm, so that $\alpha_c = \varepsilon_c / 2kT = eV(r = 0.48\text{nm}) / 2kT$. In all our considerations the titratable group is glutamic acid and as more base is added its side chain group loses a proton at its characteristic $pK_a = 4.25$ value. Its fractional negative charge f can be calculated from eq. 1, the dimensionless potential $eV(r)/kT$ of glutamic acid amino at distance $r = 0.48$ nm can be calculated from eq. 2.

Fibril solubility. As the effect of changing molecular interactions between β-strands on the fibril solubility, C_e, is difficult to determine experimentally, we estimate it theoretically by making use of the van't Hoff equation and the Haas-Drenth lattice model[34] for protein crystals. The integrated van't Hoff equation is given by $C_e = C_r e^{-\lambda}$ where C_r is a practically temperature independent reference concentration and $\lambda = L/kT$ is the dimensionless latent heat of peptide aggregation

into β-sheets. Here L is the latent heat of peptide aggregation into such aggregates. In the Haas-Drenth lattice model[34] for protein crystals λ is half the dimensionless binding energy of a peptide in an aggregate, that is $\lambda = 2\psi + 2\psi_h$. The fibril solubility is then given by

$$C_e = C_r e^{-2(\psi+\psi_h)} \tag{6}$$

Both theoretical considerations[31] and a computer-simulated peptide solubility diagram[35-37] reveal that for the irreversible elongation of differently thick amyloid fibrils (i.e. fibrils composed of different number of β-sheet layers), thermodynamics requires different ranges of the concentration C_1 of monomeric peptides (β-strands) in the solution, see Fig. 2. These ranges are limited by the equilibrium concentration (or solubility) C_e of the bulk fibrillar phase and the increasingly higher equilibrium concentrations (or solubilities) $C_{1\beta}$, $C_{2\beta}$, $C_{3\beta}$, etc. of the fibrils constituted of one β-sheet of any length, two β-sheets of any length, three β-sheets of any length, etc., respectively. Hereafter, a fibril of i β-sheets will be denoted as $i\beta$-sheet. The solubilities are merely the C_1 values at which the respective $i\beta$-sheets neither lengthen nor dissolve, and $C_{i\beta}$ is related to C_e by the expression [31] ($i = 1, 2, 3, \ldots$)

$$C_{i\beta} = C_e e^{2\psi_h/i} \tag{7}$$

The $C_1 > C_{1\beta}$ range corresponds to metanucleation, a process of fibril formation without energy barrier, because then each protein monomer (i.e. single β-strand) in the solution acts as fibril nucleus as attachment of another monomer to it allows irreversible elongation.

When $C_1 > C_{2\beta}$, 2β-sheets can lengthen irreversibly. Importantly, in the $C_{2\beta} < C_1 < C_{1\beta}$ range the 1β-sheets tend to dissolve and their appearance is due to fluctuations. In this range the fibril nucleus is a 1β-sheet plus one β-strand attached to the 1β-sheet side so that a fibril prenucleus is any of the randomly formed, differently long 1β-sheets in the solution. The situation is analogous with the 3β-sheets, the general rule is that in the ranges [31] ($i = 0, 1, 2, 3\ldots$)

$$C_e e^{2\psi_h/(i+1)} < C_1 < C_e e^{2\psi_h/i} \tag{8}$$

all differently long $i\beta$-sheets are fibril prenuclei, and these sheets plus one β-strand attached to one of their two sides are the nuclei of the $(i+1)\beta$-sheet-thick fibrils that can lengthen irreversibly.

Nucleation rate. Which fibrils form in a protein solution, and how fast, is determined by the nucleation rate J (m^{-3} s^{-1}). Experiments on protein aggregation are often performed at fixed temperature T, and based on the phase diagram discussed above we can write down expressions for J in the nucleation and metanucleation ranges. The concentration C_1 dependence of the nucleation rate in the metanucleation range (range $i = 0$) in which each monomer in the solution acts as a fibril nucleus is given by [27] ($C_1 > C_{1\beta}$)

$$J = A_1 C_1^2 \left(1 - A_2 C_1^{-1}\right) \tag{9}$$

where $A_1 = 2k_e / C_e$, $A_2 = C_e e^{2\psi_h}$, k_e is the attachment frequency of monomers to one of the two hydrogen-bond sides of a given monomer at equilibrium, C_e is the fibril solubility, and the threshold concentration $C_{1\beta}$ is obtained from eq. 7 with $i = 1$ and is given by

$$C_{1\beta} = C_e e^{2\psi_h} \tag{10}$$

The formula for J in the ith nucleation range is given by [27] ($i = 1, 2, 3, \ldots$)

$$J = A_1 C_1^{i+2} \frac{1 - A_2 C_1^{-1}}{\left(1 - A_3 C_1^{i}\right)^2} \tag{11}$$

with $A_1 = \left(4k_e / C_e^{i+1}\right) e^{-2\psi i}$, $A_2 = C_e e^{2\psi_h/(i+1)}$ and $A_3 = C_e^{-i} e^{2\psi_h}$ in the supersaturation ranges given in eq (8).

RESULTS

Our model peptide (Fig. 1) is composed of 10 amino acids only one of which has a titratable group (glutamic acid). Changing the solution conditions (pH, salt concentration, and solvent) will affect the interactions between the glutamic acids in neighbouring β-strands within the fibril and in turn the fibril nucleation rate. The application of our theoretical framework to calculate the concentration dependence of the nucleation rate follows a three-step recipe: Step 1 is to calculate the dimensionless specific surface energies ψ and ψ_h from eqs. 4 and 5. This requires knowledge of the conformation of the peptide within the fibril as they determine the number, n, of bonds between the amino acids, and the associated binding energies; Step 2 is the calculation of the fibril solubility C_e from eq. 6, which requires knowledge of the

solubility C_r of a fibril that serves as a reference. Step 3 is the calculation of the nucleation rate J from eqs. 9 and 11 which requires knowledge of the elongation rate, k_e.

Effect of solution pH

As mentioned in the introduction, solution pH can strongly affect the fibrillation rate. In our model peptide, with increasing pH the side chain group of the glutamic acid loses a proton at its characteristic pK_a = 4.25 value and becomes increasingly negatively charged. Its fractional negative charge f can be calculated from eq. 1 (see Fig. 3) and the distance dependence of the Debye Hueckel potential (eq. 2) describing the repulsive interaction between glutamic acid in water at pH = 3, 4.5 and 7 is shown in Fig. 4(a). The values used to obtain this figure are $\lambda_B = 0.7$ nm (calculated for water with a dielectric constant $\varepsilon_r = 80$ at $T = 300$ K) and $\lambda_D = 1$ nm for 100 mol/m^3 (100 mM) salt in water. The corresponding pH dependence of the dimensionless specific surface energies per amino acid, α_c, as defined above is illustrated in Fig. 4(b). As can be seen from the figure, with increasing pH the value of α_c increases and the interaction energy becomes increasingly repulsive. The values of α_c obtained at pH = 3, 4.5, and 7 are 0.04, 0.44, and 0.69, respectively. Step 1 of the recipe is to calculate the dimensionless specific surface energies from eqs. 4 and 5 which yields ψ = 11, 10.7, and 10.5 and ψ_h = 1, 0.7, and 0.5 at pH = 3, 4.5 and 7, respectively (see Fibril model for the n values used). Step 2 of the recipe is to calculate the fibril solubility C_e and its pH dependence. This can easily be done by assuming that $C_e = 6.0 \times 10^{21}$ m^{-3} (= 10 μM) for a completely uncharged peptide (see, e.g., Ref. [38]). Then eqs. 4 and 5 can be used to calculate $\psi = 11$ and $\psi_h = 1$ (for the uncharged peptide), and to obtain $C_r = 1.6 \times 10^{32}$ m^{-3} from eq. 6. Assuming that the reference concentration is independent of pH, and using it together with the values for ψ and ψ_h (for the charged peptide) in eq. 6, yields $C_e = 6.6 \times 10^{21}$ m^{-3} (= 11 μM), 1.9×10^{22} m^{-3} (= 32 μM), and 3.7×10^{22} m^{-3} (= 61 μM) at pH = 3, 4.5, and 7, respectively. Fig. 5a illustrates that C_e increases with pH, implying that with increasing pH (i.e. charge) the fibril becomes more soluble. Using a typical value for the elongation rate, $k_e = 10^4$ s^{-1} (see, e.g. Knowles et al. [39]), and assuming that it is

independent of pH, allows us to calculate the $J(C_1)$ dependence from eqs. 9 and 11 (step 3 of the recipe). As can be seen from Fig. 5b, the characteristic feature of the $J(C_1)$ dependence is a sharp rise at the transition concentrations, $C_{i\beta}$, over a narrow concentration range. For example the rise at the nucleation/metanucleation border $C_{1\beta}$ is more than 5 orders of magnitude, which is of particular relevance as for $C_1 < C_{1\beta}$ fibril nucleation becomes biologically irrelevant because only one fibril can be nucleated within a day in a volume of $\sim 1 \mu m^3$ comparable to the volume of a cell. Importantly, the main effect of increasing the pH is to shift $C_{1\beta}$ to higher concentrations and to hamper protein fibrillation because metanucleation commences at higher concentrations (see Fig. 5b). Using the C_e values from above, the threshold concentrations at pH = 3, 4.5 and 7 are $C_{1\beta} = 4.8 \times 10^{22}$ m^{-3} (= 80 μM), $C_{1\beta} = 7.9 \times 10^{22}\, m^{-3}$ (= 132 μM), and $C_{1\beta} = 1.1 \times 10^{23}\, m^{-3}$ (= 181 μM), respectively (Fig. 5a).

Our finding that increasing the overall charge of the peptide hampers protein fibrillation is in agreement with the experimental work by Carrick et al. [19] in which they used the important role of charge to design peptides for which pH can be used as a reversible switch for the formation of hydrogels. One of the peptides they considered (P11-4) is composed of 11 amino acids including Arginine at position 3 and glutamic acid at positions 5, 7, and 9. It has a net charge of +1 from the Arginine at pH < 3, but with increasing pH the Glutamic acids become increasingly protonated so that the net charge of the peptide is -2 at pH > 8. For this peptide the fibrillar gel is stable at low pH (corresponding to a low net charge) and becomes unstable at higher pH (corresponding to a higher net charge), see Fig. 1a of Ref. (21). Our findings also agrees with the work by Sammas et al. [40] on insulin where they show that insulin fibrils disaggregate with increasing charge on the protein. It also agrees with the observation that the concentration above which monomeric peptides (of sequence FEFEFKFK) aggregate correlates with their overall charge [16].

We emphasise, that in these considerations we have assumed that the pKa value of glutamic acid is not affected by the solution pH. When discussing the effect of solvent below, it will become clear that changes in pKa values can have drastic effects on the fibril nucleation rate. Consequences of changes in pKa with pH will be revisited in the DISCUSSION.

Effect of salt concentration

Adding salt to a solvent shields the electrostatic interaction between charged species in the solution. The main effect of changing the salt concentration on the columbic interaction between the glutamic amino acids is to change the Debye screening length λ_D, while we assume that the Bjerrum length λ_B and the pK_a value are not affected. Reducing the salt concentration from 100 mol/m^3 (100 mM) to 1 mol/m^3 (1 mM) salts in water increases λ_D from 1 nm to 10 nm. The effect of this increase on the distance dependence of the Debye Hueckel potential from eq. 2 describing glutamic acid in water and the dimensional specific surface energy per amino acid α_c are shown in Fig. 4 by the dashed lines. Decreasing the salt concentration increases the repulsion between two charged amino acids, and this effect becomes stronger with increasing pH. The values of α_c obtained at pH = 3, 4.5, and 7 are 0.02, 0.29, and 0.45, respectively. In order to calculate the effect of salt concentration on the $J(C_1)$ dependence we calculate ψ and ψ_h (step 1 of recipe). From Eqs 4 and 5 we obtain that $\psi = 11.0$, 10.6, and 10.3 and ψ_h = 1.0, 0.6, and 0.3 each at pH = 3, 4.5, and 7, respectively. Step 2 of the recipe is to calculate the pH dependence of the solubility. Assuming that $C_r = 1.6\times10^{32}$ m^{-3} is again independent of pH and salt concentration, and with the ψ and ψ_h values above, we obtain from eq. 6 that $C_e = 7.2\times10^{21}$ m^{-3} (= 12 μM), 3.6×10^{22} m^{-3} (= 59 μM), and 9.6×10^{22} m^{-3} (= 160 μM), at pH = 3, 4.5, and 7, respectively. As can be seen from Fig. 5a, the increase with pH in the value of C_e is more pronounced when less salt is present. As in the previous example, the $J(C_1)$ dependence at different pH values is obtained from eqs. 9 and 11 with $k_e = 10^4$ s^{-1}. Fig. 5b shows that the shift of $C_{1\beta}$ to higher concentrations is even more pronounced when less salt is present, which hampers protein fibrillation even more. Using the C_e values from above, the threshold concentrations obtained from eq. 10 at pH = 3, 4.5 and 7 are $C_{1\beta} = 4.8\times10^{22}$ m^{-3} (= 80 μM), 1.1×10^{23} m^{-3} (= 179 μM), and 1.8×10^{23} m^{-3} (= 296 μM), at pH = 3, 4.5, and 7, respectively. Our finding that adding salt decreases the fibril solubility and increases the nucleation rate is consistent with the experimental observation by Carrick et al. [19] that the transition range in which fibrillar gels form and are stable is shifted to higher pH values (at which the peptide has a

higher charge to compensate for the higher salt concentration and screening between the charged residues). Also, in the work by Hoyer et al. [10] on α-synuclein they found that with increasing pH aggregation lag time increases.

Effect of solvent

The main effect of changing the solvent from e.g. water to a less polar solvent is that the dielectric constant ε_r decreases. This affects the electrostatic interaction between two charged amino acids, as in the expression from Debye Hueckel theory eq. 2 the Bjerrum length increases and the Debye length decreases with decreasing ε_r (see Fig. 6a). The combined effect on the Debye-Hueckel potential calculated at pH = 4.5 is that the electrostatic screening is more effective in polar solvents like water compared to non-polar ones (Fig. 7a). The corresponding decrease of the dimensionless specific surface energies per amino acid due to columbic bonding, α_c, is shown in Fig. 7b. In order to calculate the effect of solvent on the $J(C_1)$ dependence we first calculate the ψ and ψ_h (step 1 of recipe) at different values for the dielectric constant. For $\varepsilon_r = 80$, 50 and 20 and 100mM salt concentration, the values for the Debye length are $\lambda_D = 1.0$ nm, 0.8 nm, 0.5 nm and for the Bjeruum length are $\lambda_B = 0.7$ nm, 1.1 nm, 2.8 nm, respectively. The corresponding values of α_c obtained for $\varepsilon_r = 80$, 50 and 20 are 0.28, 0.40, and 0.69, respectively. Using these values in eqs 4 and 5 we obtain that $\psi = 10.7$, 10.6, and 10.3 and ψ_h = 0.7, 0.6, and 0.3 each at $\varepsilon_r = 80$, 50, and 20, respectively. Step 2 of the recipe is to calculate the pH dependence of the solubility. Assuming that $C_r = 1.6 \times 10^{32}$ m^{-3} is independent of the solvent, and with the ψ and ψ_h values above, we obtain that $C_e = 2 \times 10^{22}$ m^{-3} (= 31 μM), 3×10^{22} m^{-3} (= 49 μM), and 10×10^{22} m^{-3} (= 160 μM), at $\varepsilon_r = 80$, 50, and 20, respectively. As can be seen from Fig. 8a, increasing the dielectric constant decreases C_e and the fibrils are less soluble. As in the previous example, we calculate the $J(C_1)$ dependence at different pH values from eqs. 9 and 11 with $k_e = 10^4$ s^{-1}. Fig. 8b shows that the main effect of increasing ε_r is to shift the threshold concentration $C_{1\beta}$ to lower concentrations and to promote protein fibrillation. Using the C_e values from above, the threshold concentrations for $\varepsilon_r = 80$, 50 and 20 are $C_{1\beta} = 8 \times 10^{22}$ m^{-3} (=

130 μM), 10×10^{22} m^{-3} (= 164 μM), and 17×10^{22} m^{-3} (= 296 μM), respectively. Interestingly, the prediction that increasing dielectric constant decreases fibril solubility and promotes fibrillation is in contrast to experimental observations (see e.g. Ref. [41]).

In order to resolve this discrepancy, it is necessary to consider the fact that the pKa value of the charged residue also depends on the solvent (see Methods). To estimate this effect we are considering glutamic acid in water (with $\varepsilon_r = 80$ and $pK_a = 4.25$) as a reference solute solvent at T = 300 K, and using eq. 3 with ($a_+ + a_-$) = 0.35 nm as a diameter for the OH group, predicts that the pKa values decrease with increasing dielectric constant (see Fig. 6b), for example $pK_a = 5.54$, 4.51 and 4.25 at $\varepsilon_r = 20$, 50, and 80, respectively.

The higher pKa values in less polar solvents leads to a cascade of effects, it decreases the fraction of the ionised side-chain group of glutamic acid, which leads to a decrease in the electrostatic repulsion between charged amino acids, which leads to a decrease in the dimensionless specific surface energy per amino acid due to columbic bonds and the corresponding values for the dimensionless specific surface energies, which in turn lowers the fibril solubility and the threshold concentration and hence promotes protein fibrillation.

In the considerations above we found that at pH = 4.5 and salt concentration 100 mM the solubility of fibrils in water with $\varepsilon_r = 80$ is $C_e = 2\times10^{22}$ m^{-3} (= 31 μM), and that replacing water with a solvent with $\varepsilon_r = 20$ leads to a solubility of $C_e = 10\times10^{22}$ m^{-3} (= 160 μM), see also Fig. 8a. However, considering that the pKa value of glutamic acid increases to 5.54 (from 4.25 in water) leads to a decreased electrostatic repulsion and α_c decreases to 0.09 (from 0.69 in water), see Fig. 7 dashed lines. In these calculations we have used $\lambda_D = 0.5$ nm and $\lambda_B = 2.8$ nm from above, as they are independent of the pKa value. Using the so obtained values in eqs 4 and 5 yields the corresponding values for dimensionless specific surface energies $\psi = 10.9$ and ψ_h = 0.9. Assuming again that $C_r = 1.6\times10^{32}$ m^{-3} is independent of the pKa value, the solubility is $C_e = 9\times10^{21}$ m^{-3} (= 14 μM), which is much lower than the solubility in water (Fig. 8a). As before, the $J(C_1)$ dependence with $k_e = 10^4$ s^{-1} is obtained from eqs. 9 and 11, and Fig. 8b shows that with a higher value of pKa, the

threshold concentration $C_{1\beta}$ is shifted to lower concentrations and protein fibrillation is much enhanced. Using the C_e values from above, the threshold concentration is $C_{1\beta} = 5 \times 10^{22}$ m^{-3} (= 88 μM).

The main result from these considerations is that an increase of the pKa value opposes the effect of the reduced dielectric constant, and this effect can dominate so that the fibril nucleation rate can be enhanced in less polar solvents (see Fig.8b) in line with experimental observations (see e.g. Ref. [41]). This effect is more pronounced for solution conditions at which the fractional charge of the residue is large, i.e in this example at higher pH values. In the limiting case where the shift of the pKa value increases such that the fractional charge of the residue approaches zero, the nucleation rate will be identical to that of an uncharged system, i.e. close to that of the nucleation rate shown in Fig. 5b at pH = 3.

DISCUSSION

Main results. The main results from this study are that (i) increases in solution pH that increase the net charge of the peptide make fibrils more soluble and hamper protein fibrillation; (ii) increasing the salt concentration decreases the solubility of fibrils and promotes protein fibrillation; (iii) changing the solvent from water to a more polar one increases the solubility of the fibrils and hampers protein fibrillation. Importantly, when considering the effect of an increased pKa value of glutamic acid in polar solvents will lower the fibrils solubility and promote protein fibrillation. The latter of these two opposing effects can dominate, so that fibril nucleation can be enhanced in less polar solvents.

Importance of fibril solubility and threshold concentration. As in our previous work [29], the results obtained highlight the important role of the fibril solubility C_e and the threshold $C_{1\beta}$ concentration in amyloid fibril nucleation. Substitution of eqs. 4 and 5 into eq. 6

$$C_e = C_r e^{-2(\psi+\psi_h)} = C_r e^{-(n\varepsilon+2n_h\varepsilon_h-2n_c\varepsilon_c)/kT} \qquad (12)$$

allows us to express the solubility in terms of the binding energy between neighboring β-strands in the fibril, and substitution of eqs. 4 and 5 into Eq. 10 yields the corresponding expression for the threshold concentration

$$C_{1\beta} = C_e e^{2\psi_h} = C_r e^{-(n\varepsilon + n_h \varepsilon_h - n_c \varepsilon_c)/kT} . \qquad (13)$$

These two simple analytical expressions, in combination with the Debye Hueckel theory eq. 2, allow us to rationalize the results obtained.

Increases in solution pH, that increase the net charge and thereby ε_c, increase C_e (as can be seen from eq. 12) and fibrils become more soluble. The increase in ε_c also increases $C_{1\beta}$ (as can be seen from eq. 13) which hampers proteins fibrillation because metanucleation commences at higher concentrations. Increasing the salt concentration lowers ε_c which decreases C_e (as can be seen from eq. 12) and fibrils become less soluble. The decrease in ε_c also decreases $C_{1\beta}$ (which can be seen from eq. 13) which promotes proteins fibrillation because metanucleation commences at lower concentrations. Changing water to a more polar solvent decreases the dielectric constant ε_r which in turn increases ε_c and increases C_e (see eq. 12) and fibrils become more soluble. Increasing ε_c increases $C_{1\beta}$ (see eq. 13) which hampers proteins fibrillation. Considering that the pKa value increase in non polar solvent opposes this effect as ε_c decreases, and eqs. 12 and 13 show that in turn C_e and $C_{1\beta}$ decrease and protein fibrillation is promoted.

The general rule that emerges from these considerations is that changes in the solution conditions that increase the bonding energy of peptides in the fibril decrease the fibril solubility and promote amyloid fibril nucleation. The general rule is in accord with our recent results [29] on amyloid polymorphism where changes in the conformation of the fibril building blocks or their packing that increase their binding energy decrease fibril solubility and promote protein fibrillation. The results presented in this study further illustrates the power of our theoretical framework which provides a tool to qualitatively and quantitatively predict effects of amino acid sequence, polymorphism and solvent based on the fundamental interactions between the fibril building blocks.

Experimental verification. A verification of our results of the effect on solution conditions on amyloid fibril nucleation requires a direct measurement of the fibril nucleation rate. At present, the numerous experimental studies are mainly for the lag time and maximal rate of overall aggregation. Time-resolved optical experiments that measure the fluorescence signal arising from dye molecules such as

thioflavin T bound to the protein aggregates enable determination of lag time and the maximal rate of overall aggregation. This type of experiments does not allow a reliable determination of *J*, as it is well know that it depends on other factors such as solution agitation, detection limit, because post-nucleation processes such as fragmentation can affect the overall aggregation process.

It is worth noting that some generalized rate equations[42,43] commonly used to analyze time-resolved optical experiments describing the fibrillation kinetics contain a semiempirical quantity called the fibril nucleation rate introduced ad hoc, which does not correspond to the nucleation rate as obtained in classical nucleation theory[44]. A precise method of experimentally obtaining an estimate of the nucleation rate is to measure the probability to form at least one fibril of a given size as a function of time[45].

Effect of pH on pKa value. A very important point in our discussions of the effect of pH and salt on the fibril nucleation rate is that we assumed that the pKa value does not depend on pH. With increasing pH the fraction of ionized glutamic acids in solution increases and the remaining ones should bind their protons more strongly due to the increased electro-negative environment, resulting in a rise in their pKa value. This effect has been seen in other protein systems, like the tetrameric M2 proton channel[46] where instead of seeing cooperative deprotonation of all 4 histidine side chains at pH 6 (the pKa value of isolated histidine), the pKa values range from 5 to above 8. In absence of an analytical theory describing the effect of pH on the pKa value on glutamic acid, we can only qualitatively predict that an increase of the pKa value with pH opposes the effect of pH on the nucleation rate discussed above (Fig. 5) and will promote protein fibrillation, similar to the effect of solvent on the pKa value discussed above (Fig. 8b). In the limiting case when the pKa value increase such that the fractional charge of the residue approaches zero, the nucleation rate becomes that of an uncharged system (i.e close to the rate shown in Fig. 5b at pH = 3).

CONCLUSIONS

We conclude that the combination of our newly developed nonstandard nucleation theory with Debye Hueckel theory to describe the interactions between the fibril building blocks can be used to predict the concentration dependence of the nucleation rate at different pH, salt concentration and solvent. The general rule that emerges

from these considerations is that changes in the solution conditions that increase the bonding energy of peptides in the fibril decrease the fibril solubility and promote amyloid fibril nucleation. Our results highlight the important role of the fibril solubility C_e and the threshold $C_{1\beta}$ concentration in amyloid fibril nucleation and eq. 12 and 13 allow us to rationalise the results obtained. The analytical relations between the nucleation rate, the fibrils solubility and the binding energies between the fibril building blocks might prove a valuable tool how to control amyloid fibril formation by changing the solution conditions.

ACKNOWLEDGEMENTS

The author thanks Professor Paul P.A.M. van der Schoot and Professor Dimo Kashchiev for stimulating discussions during the course of this study and for their comments on the manuscript.

FIGURES

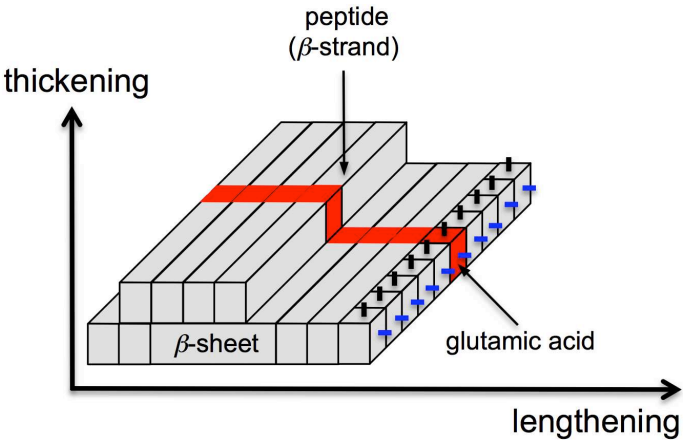

Fig. 1. Illustration of an amyloid fibril (2β-sheet) composed of two β-sheets one of which is constituted of 9 peptides (bottom β-sheet) and the other of 4 peptides (top β-sheet). In the fibril model each peptide is in an extended β-strand conformation and composed of 10 amino acids (cubes), only one of which is a titratable group (shown in red). The peptides within the fibril are arranged parallel to each other and each amino acid can form bonds (visualised by the red and blue lines) with nearest neighbour amino acids only. See Method for a detailed description of the model.

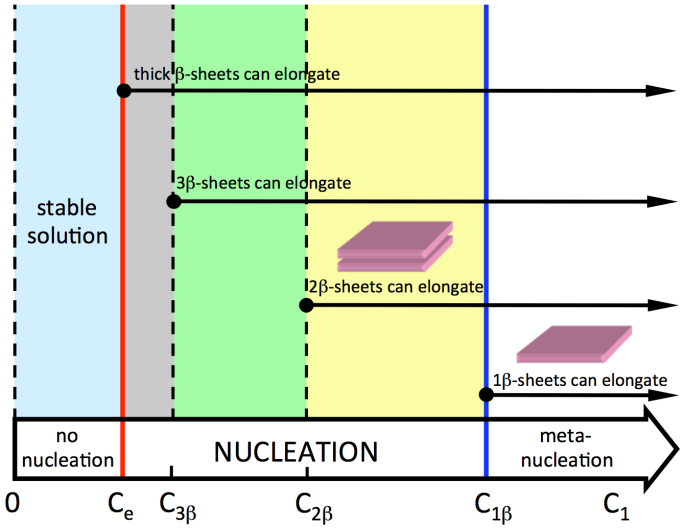

Fig. 2. Monomer concentration ranges determined by the fibril solubility C_e, the metanucleation border $C_{1\beta}$, and intermediate concentrations $C_{i\beta}$ for $i \geq 2$.

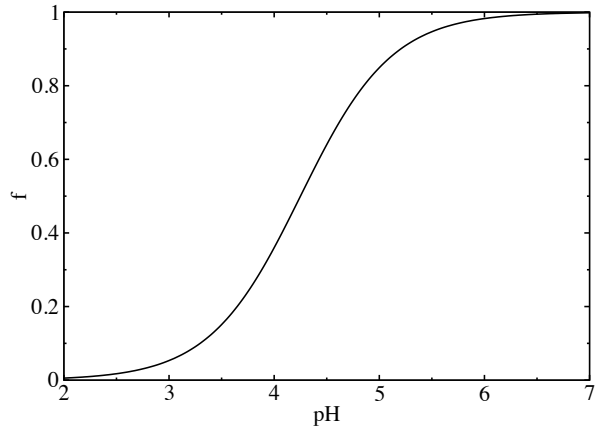

Fig. 3. pH dependence of the fraction *f* of the (negatively charged) ionised side-chain group of glutamic acid obtained from eq. 1 with $pK_a = 4.25$.

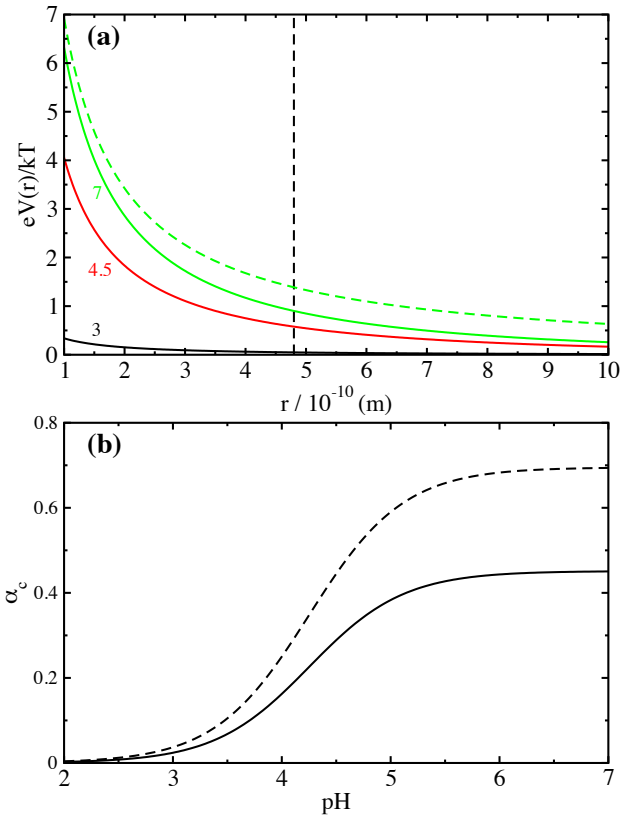

Fig. 4. (a) Distance dependence of Debye Hueckel potential from eq. 2 describing glutamic acid in water with $pK_a = 4.25$ at pH = 3, 4.5 and 7 as indicated. The vertical dashed black line is at a hydrogen bonding distance $r = 4.8$ nm. The Bjerrum length used in this plot is $\lambda_B = 0.7$nm, and the Debye lengths used are $\lambda_D = 10$ nm (dashed line, 1 mol/m^3) and 1 nm (solid lines, 100 mol/m^3), respectively. (b) Corresponding pH dependence of the dimensionless specific surface energies per amino acid, α_c, due to columbic bonds. The dashed and solid lines are obtained for salt concentrations 1 mol/m^3 and 100 mol/m^3, respectively.

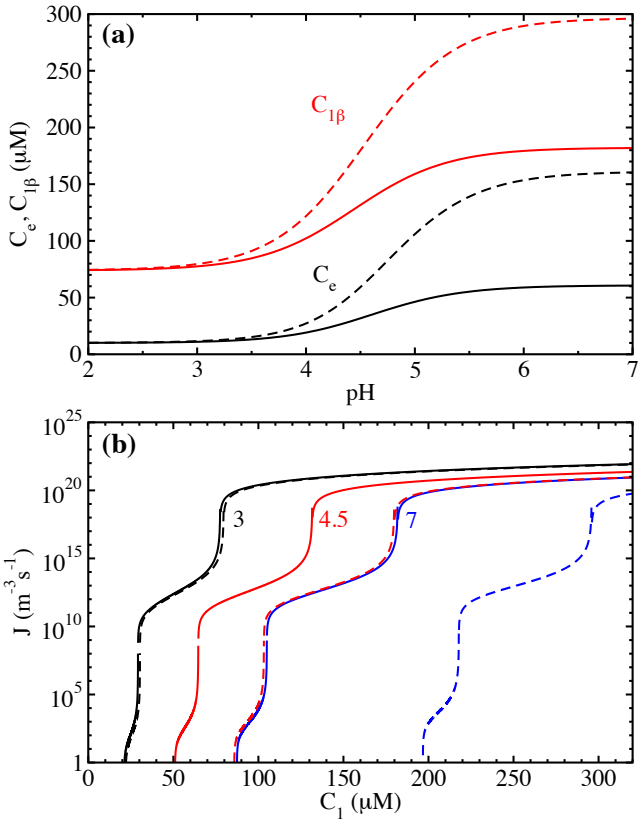

Fig. 5. (a) Dependence of the fibril solubility C_e and threshold concentration $C_{1\beta}$ on pH in water and pKa = 4.25. (b) Concentration dependence of the nucleation rate at pH = 3, 4.5 and 7 as indicated. As in Figure 4, the value for the Bjerrum length used is λ_B = 0.7 nm and the Debye lengths are λ_D = 1 nm (dashed lines, 1 mol/m^3) and 10 nm (solid lines, 100 mol/m^3), respectively.

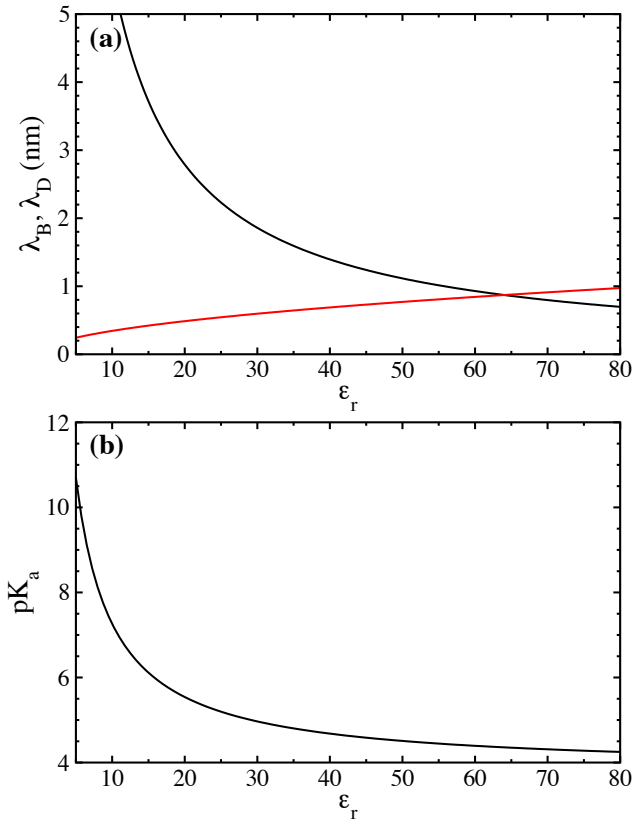

Fig. 6. (a) Dependence of the Debye length λ_D (red line) and Bjerrum length λ_B (black line) on dielectric constant obtained at T = 300K and salt concentration 100mM. (b) Dependence of the pK_a value of glutamic acid on the dielectric constant ε_r, obtained from eq.3.

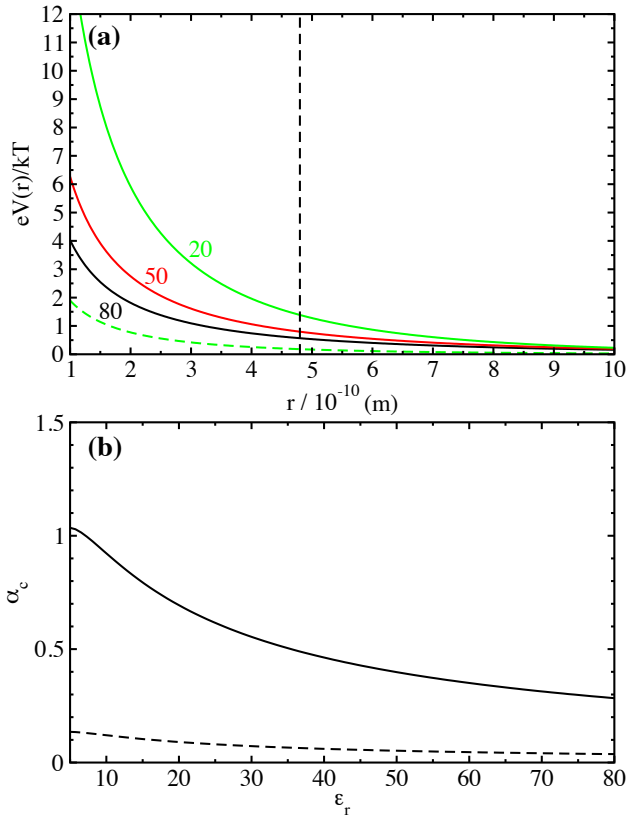

Fig. 7. (a) Distance dependence of Debye Hueckel potential at $\varepsilon_r = 80$, 50 and 20 as indicated at pH = 4.5. The solid lines have been calculated for pKa = 4.25 and the dashed line has been calculated for pKa = 5.54. The vertical dashed black line is at a hydrogen bonding distance r = 0.48 nm. (b) The dimensionless specific surface energies per amino acid α_c (which is equal to half the value of the Debye Hueckel potential at hydrogen bonding distance r = 0.48 nm) as a function of ε_r. The solid and dashed lines have been calculated for pKa = 4.25 and 5.54, respectively.

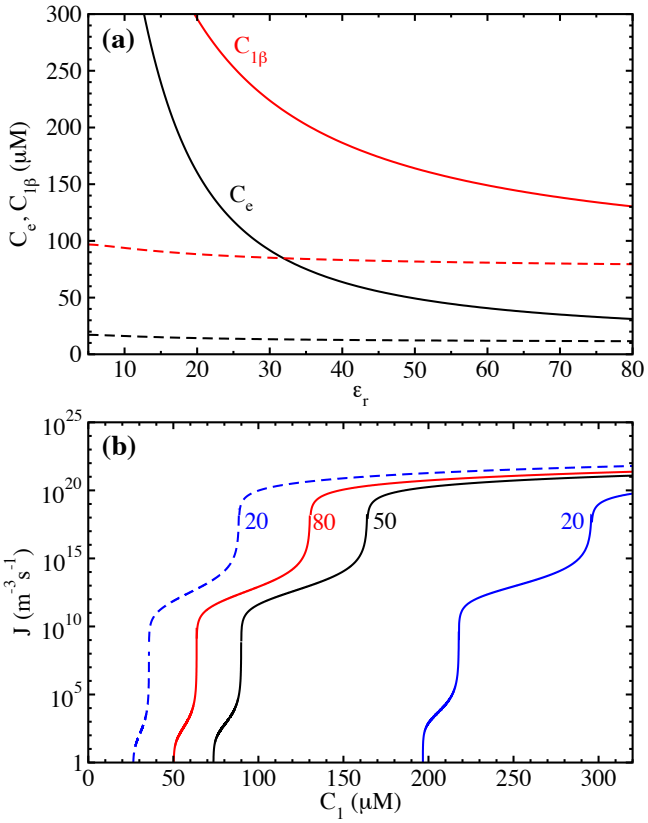

Fig. 8. (a) Dependence of the fibril solubility (black lines) and the threshold concentration (red lines) on the dielectric constant ε_r at pH = 4.5. The solid and dashed lines correspond to pKa values of 4.25 and 5.54, respectively. (b) Concentration dependence of the nucleation rate at $\varepsilon_r = 80$ (red), 50 (black) and 20 (blue) at pH = 4.5. The solid and dashed lines correspond to pKa values of 4.25 and 5.54, respectively.

REFERENCES

1. Cherny, I.; Gazit, E. Amyloids: Not Only Pathological Agents But Also Ordered Nanomaterials. *Angew Chem Int Edit* **2008**, *47*, 4062-4069.
2. Barrow, C. J.; Zagorski, M. G. Solution Structures of Beta Peptide and Its Constituent Fragments - Relation to Amyloid Deposition. *Science* **1991**, *253*, 179-182.
3. Snyder, S. W.; Ladror, U. S.; Wade, W. S.; Wang, G. T.; Barrett, L. W.; Matayoshi, E. D.; Huffaker, H. J.; Krafft, G. A.; Holzman, T. F. Amyloid-Beta Aggregation - Selective-Inhibition of Aggregation in Mixtures of Amyloid with Different Chain Lengths. *Biophys J* **1994**, *67*, 1216-1228.
4. Wood, S. J.; Maleeff, B.; Hart, T.; Wetzel, R. Physical, Morphological and Functional Differences Between pH 5.8 and 7.4 Aggregates of the Alzheimer's Amyloid Peptide AP. *J Mol Biol* **1996**, *256*, 870-877.
5. Fraser, P. E.; Nguyen, J. T.; Surewicz, W. K.; Kirschner, D. A. pH-Dependent Structural Transitions of Alzheimer Amyloid Peptides. *Biophys J* **1991**, *60*, 1190-1201.
6. McParland, V. J.; Kad, N. M.; Kalverda, A. P.; Brown, A.; Kirwin-Jones, P.; Hunter, M. G.; Sunde, M.; Radford, S. E. Partially Unfolded States of Beta(2)-microglobulin and Amyloid Formation in Vitro. *Biochemistry* **2000**, *39*, 8735-8746.
7. Ratnaswamy, G.; Koepf, E.; Bekele, H.; Yin, H.; Kelly, J. W. The Amyloidogenicity of Gelsolin is Controlled by Proteolysis and pH. *Chem Biol* **1999**, *6*, 293-304.
8. Chiti, F.; Bucciantini, M.; Capanni, C.; Taddei, N.; Dobson, C. M.; Stefani, M. Solution Conditions can Promote Formation of Either Amyloid Protofilaments or Mature Fibrils from the HypF N-terminal Domain. *Protein Sci* **2001**, *10*, 2541-2547.
9. Lai, Z. H.; Colon, W.; Kelly, J. W. The Acid-mediated Denaturation Pathway of Transthyretin Yields a Conformational Intermediate that can Self-assemble into Amyloid. *Biochemistry* **1996**, *35*, 6470-6482.
10. Hoyer, W.; Antony, T.; Cherny, D.; Heim, G.; Jovin, T. M.; Subramaniam, V. Dependence of Alpha-synuclein Aggregate Morphology on Solution Conditions. *J Mol Biol* **2002**, *322*, 383-393.
11. Zurdo, J.; Guijarro, J. I.; Jimenez, J. L.; Saibil, H. R.; Dobson, C. M. Dependence on Solution Conditions of Aggregation and Amyloid Formation by an SH3 Domain. *J Mol Biol* **2001**, *311*, 325-340.
12. Alexandrescu, A. T.; Rathgeb-Szabo, K. An NMR Investigation of Solution Aggregation Reactions Preceding the Misassembly of Acid-denatured Cold Shock Protein A into Fibrils. *J Mol Biol* **1999**, *291*, 1191-1206.
13. Srinivasan, R.; Jones, E. M.; Liu, K.; Ghiso, J.; Marchant, R. E.; Zagorski, M. G. pH-dependent Amyloid and Protofibril Formation by the ABri Peptide of Familial British Dementia. *J Mol Biol* **2003**, *333*, 1003-1023.
14. Buell, A. K.; Galvagnion, C.; Gaspar, R.; Sparr, E.; Vendruscolo, M.; Knowles, T. P. J.; Linse, S.; Dobson, C. M. Solution Conditions Determine the Relative Importance of Nucleation and Growth Processes in Alpha-synuclein Aggregation. *P Natl Acad Sci USA* **2014**, *111*, 7671.
15. McGlinchey, R. P.; Jiang, Z. P.; Lee, J. C. Molecular Origin of pH-Dependent Fibril Formation of a Functional Amyloid. *Chembiochem* **2014**, *15*, 1569-1572.
16. Boothroyd, S.; Miller, A. F.; Saiani, A. From Fibres to Networks Using Self-assembling Peptides. *Faraday Discuss* **2013**, *166*, 195-207.
17. Schmittschmitt, J. P.; Scholtz, J. M. The Role of Protein Stability, Solubility, and Net Charge in Amyloid Fibril Formation. *Protein Sci* **2003**, *12*, 2374-2378.
18. Aggeli, A.; Bell, M.; Carrick, L. M.; Fishwick, C. W. G.; Harding, R.; Mawer, P. J.; Radford, S. E.; Strong, A. E.; Boden, N. pH as a Trigger of Peptide Beta-sheet

Self-assembly and Reversible Switching Between Nematic and Isotropic Phases. *J Am Chem Soc* **2003**, *125*, 9619-9628.

19. Carrick, L. M.; Aggeli, A.; Boden, N.; Fisher, J.; Ingham, E.; Waigh, T. A. Effect of Ionic Strength on the Self-assembly, Morphology and Gelation of pH Responsive Beta-sheet Tape-forming Peptides. *Tetrahedron* **2007**, *63*, 7457-7467.

20. Chiti, F.; Stefani, M.; Taddei, N.; Ramponi, G.; Dobson, C. M. Rationalization of the Effects of Mutations on Peptide and Protein Aggregation Rates. *Nature* **2003**, *424*, 805-808.

21. Fernandez-Escamilla, A. M.; Rousseau, F.; Schymkowitz, J.; Serrano, L. Prediction of Sequence-dependent and Mutational Effects on the Aggregation of Peptides and Proteins. *Nat Biotechnol* **2004**, *22*, 13021306.

22. Tartaglia, G. G.; Pawar, A. P.; Campioni, S.; Dobson, C. M.; Chiti, F.; Vendruscolo, M. Prediction of aggregation-prone regions in structured proteins. *J Mol Biol* **2008**, *380*, 425-436.

23. Trovato, A.; Chiti, F.; Maritan, A.; Seno, F. Insight into the Structure of Amyloid Fibrils from the Analysis of Globular Proteins. *Plos Comput Biol* **2006**, *2*, 1608-1618.

24. Morris, A. M.; Watzky, M. A.; Finke, R. G. Protein Aggregation Kinetics, Mechanism, and Curve-fitting: A Review of the Literature. *Bba-Proteins Proteom* **2009**, *1794*, 375-397.

25. Cohen, S. I. A.; Vendruscolo, M.; Dobson, C. M.; Knowles, T. P. J. From Macroscopic Measurements to Microscopic Mechanisms of Protein Aggregation. *J Mol Biol* **2012**, *421*, 160-171.

26. Morriss-Andrews, A.; Shea, J. E. Computational Studies of Protein Aggregation: Methods and Applications. *Annu Rev Phys Chem* **2015**, *66*, 643-666.

27. Kashchiev, D.; Cabriolu, R.; Auer, S. Confounding the Paradigm: Peculiarities of Amyloid Fibril Nucleation. *J Am Chem Soc* **2013**, *135*, 15311539.

28. Auer, S. Amyloid Fibril Nucleation: Effect of Amino Acid Hydrophobicity. *J Phys Chem B* **2014**, *118*, 5289-5299.

29. Auer, S. Nucleation of Polymorphic Amyloid Fibrils. *Biophys J* **2015**, *108*, 1176-1186.

30. Israelachvili, J. N. *Intermolecular and Surface Forces,* Academic Press: Oxford U.K., 2011.

31. Kashchiev, D.; Auer, S. Nucleation of Amyloid Fibrils. *J Chem Phys* **2010**, *132*, 215101.

32. Fersht, A. R.; Shi, J. P.; Knilljones, J.; Lowe, D. M.; Wilkinson, A. J.; Blow, D. M.; Brick, P.; Carter, P.; Waye, M. M. Y.; Winter, G. Hydrogen-Bonding and Biological Specificity Analyzed by Protein Engineering. *Nature* **1985**, *314*, 235-238.

33. Nguyen, H. D.; Hall, C. K. Molecular Dynamics Simulations of Spontaneous Fibril Formation by Random-coil Peptides. *P Natl Acad Sci USA* **2004**, *101*, 16180-16185.

34. Haas, C.; Drenth, J. The Interaction Energy between 2 Protein Molecules Related to Physical-Properties of Their Solution and Their Crystals and Implications for Crystal-Growth. *J Cryst Growth* **1995**, *154*, 126-135.

35. Auer, S.; Kashchiev, D. Phase Diagram of alpha-Helical and beta-Sheet Forming Peptides. *Phys Rev Lett* **2010**, *104*, 168105.

36. Auer, S. Phase Diagram of Polypeptide Chains. *J Chem Phys* **2011**, *135*, 175103.

37. Rizzi, L. G.; Auer, S. Amyloid Fibril Solubility. *J Phys Chem B* **2015**, *119*, 14631-1463.

38. Aggeli, A.; Nyrkova, I. A.; Bell, M.; Harding, R.; Carrick, L.; McLeish, T. C. B.; Semenov, A. N.; Boden, N. Hierarchical Self-assembly of Chiral Rod-like Molecules as a Model for Peptide Beta-sheet Tapes, Ribbons, Fibrils, and Fibers. *P Natl Acad Sci USA* **2001**, *98*, 11857-11862.

39. Knowles, T. P. J.; Shu, W. M.; Devlin, G. L.; Meehan, S.; Auer, S.; Dobson, C. M.; Welland, M. E. Kinetics and Thermodynamics of Amyloid Formation From Direct Measurements of Fluctuations in Fibril Mass. *P Natl Acad Sci USA* **2007**, *104*, 10016-10021.

40. Shammas, S. L.; Knowles, T. P. J.; Baldwin, A. J.; MacPhee, C. E.; Welland, M. E.; Dobson, C. M.; Devlin, G. L. Perturbation of the Stability of Amyloid Fibrils through Alteration of Electrostatic Interactions. *Biophys J* **2011**, *100*, 2783-2791.

41. Davies, R. P. W.; Aggeli, A. Self-assembly of Amphiphilic Beta-sheet Peptide Tapes based on Aliphatic Side Chains. *J Pept Sci* **2011**, *17*, 107-114.

42. Michaels, T. C. T.; Garcia, G. A.; Knowles, T. P. J. Asymptotic Solutions of the Oosawa Model for the Length Distribution of Biofilaments. *J Chem Phys* **2014**, *140*, 194906.

43. Michaels, T. C. T.; Liu, L. X.; Meisl, G.; Knowles, T. P. J. Physical Principles of Filamentous Protein Self-assembly Kinetics. *J Phys-Condens Mat* **2017**, *29*, 153002.

44. Kashchiev, D. Protein Polymerization into Fibrils from the Viewpoint of Nucleation Theory. *Biophys J* **2015**, *109*, 2126-2136.

45. Kashchiev, D. Modeling the Effect of Monomer Conformational Change on the Early Stage of Protein Self-Assembly into Fibrils. *J Phys Chem B* **2017**, *121*, 35-46.

46. Hu, J.; Fu, R.; Nishimura, K.; Zhang, L.; Zhou, H. X.; Busath, D. D.; Vijayvergiya, V.; Cross, T. A. Histidines, Heart of the Hydrogen Ion Channel from Influenza A Virus: Toward an Understanding of Conductance and Proton Selectivity. *P Natl Acad Sci USA* **2006**, *103*, 6865-6870.

TOC

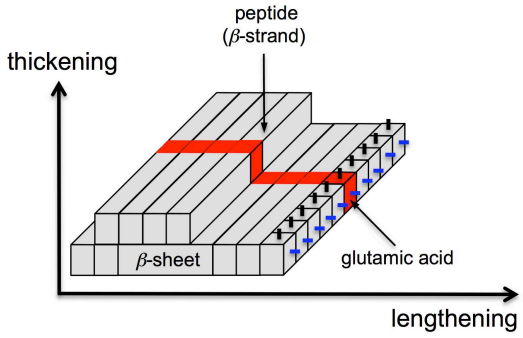
peptide
(β-strand)
thickening
β-sheet
glutamic acid
lengthening